Research on the Effect of Heat Pipe Inclination Angle on Temperature Distribution in Electrical Machines

Han Zhao, Xiaochen Zhang, *Member, IEEE*, Jing Li, *Senior Member, IEEE*, Fengyu Zhang, *Member, IEEE*, Yue Zhang, Hongyu Yan, Xiaorui Zhu, Zhihao Niu, David Gerada, *Senior Member, IEEE*

***Abstract*—Due to high equivalent thermal conductivity with lightweight and small size, heat pipes (HPs) are being extensively applied in the motor cooling system to improve its thermal performance. However, when practically installed in electrical machines, the inclination angle of the HP will affect its thermal conductivity and motor temperature distribution as well, which is still unclear. This article intends to figure out the effects of HP inclination angle on motor temperature distribution via both theoretical and experimental investigation. Based on the theoretical analysis of the HP inclination effect, the equivalent thermal conductivity of the HP with different inclination angles from 0° to 180° is experimentally investigated on a dedicated platform. Then, temperature distribution across a full-size stator-winding assembly with HPs is quantitatively studied using an established thermal model. Finally, the thermal simulation results are experimentally verified by testing on a processed specimen. The results indicate that the HP thermal performance degrades by over 80% with the inclination angle from 0° to 180°, which results in a significant temperature nonuniformity across the motor under liquid cooling conditions.**

***Index Terms*—Cooling method, electrical machine, equivalent thermal conductivity, experimental validation, heat pipe (HP), inclination angle, temperature distribution, thermal analysis.**

I. Introduction

DUE to the depletion of fossil energy and increasingly stringent requirements on carbon emission, there has been tremendous progress in the development of transportation electrification in recent years, such as electric vehicles and more electric aircraft, which propose greater demands on the motor power density and challenges as well to its cooling system [1-5]. To address such technical issues, HPs, which have been verified with remarkable cooling effectiveness in other contexts, are being extensively explored in motor cooling scenarios to enhance cooling capacity and extend power density boundaries [6-8].

HP is a passive thermally conductive device with a compact geometry and lightweight, which enables considerable heat transmission over a long distance with a small temperature drop and the absence of external energy consumption [9]. A typical copper-water HP is composed of a hollow sealed copper shell, a sintered wick structure, and a vacuum vapor space, as illustrated in Fig. 1 [10]. The operating principle of the HP is based on the phase transition of the internal working medium, which absorbs heat during evaporation and releases heat during condensation. By the capillary force generated in the wick structure, the working medium is driven from the evaporator section back to the condenser section, which could provide a very high value of equivalent thermal conductivity of up to 100000 W/m·K considering its lightweight and small size, thereby making it a competitive cooling device for electrical machines [9].

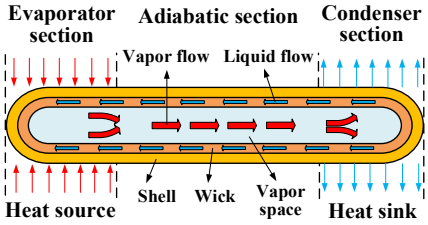

Fig. 1. Schematic of HP structure and working principle.

Due to the gravitational effect on the backflow of the working medium, the inclination angle has a significant impact on HP thermal performance, which has been confirmed by the studies in the fields of thermology and mechanical engineering [11-16]. If we define the inclination angle θ as the angle between the backflow direction and the gravity direction of the working medium, the gravitational effect on the backflow of the internal working medium in the HP can be divided into the gravity-assisted case ($\theta < 90^\circ$) and gravity-opposed case ($\theta > 90^\circ$), as shown in Fig. 2. For the gravity-assisted case, the evaporator section of the HP is lower than the condenser section, and the gravity facilitates the backflow of the liquid

This work was supported in part by the Ningbo Key Technology Research and Development Programme under Grant 2021Z035, in part by the Ministry of Science & Technology through the National Key R&D Program of China under Grant 2021YFE0108600, and in part by the Key International Cooperation of National Natural Science Foundation of China under Grant 51920105011. *(Corresponding author: Xiaochen Zhang).*

Han Zhao, Jing Li, Yue Zhang, Hongyu Yan, Xiaorui Zhu, and Zhihao Niu are with the Key Laboratory of More Electric Aircraft Technology of Zhejiang Province, University of Nottingham Ningbo China, Ningbo 315100, China (email: sgxhz1@nottingham.edu.cn; Jing.Li@nottingham.edu.cn; ssyyz27@nottingham.edu.cn; ssyhy9@nottingham.edu.cn; ssyxz8@nottingham.edu.cn; ssyzn1@nottingham.edu.cn).

Xiaochen Zhang is with the Advanced Electric Drive Centre, Yongjiang Laboratory, Ningbo 315202, China, and also the Key Laboratory of More Electric Aircraft Technology of Zhejiang Province and the Nottingham Ningbo China Beacons of Excellence Research and Innovation Institute, University of Nottingham Ningbo China, Ningbo 315100, China (email: Xiaochen.Zhang@nottingham.edu.cn).

Fengyu Zhang and David Gerada are with Power Electronics, Machines and Control Group, University of Nottingham, Nottingham NG7 2RD, U.K. (email: Fengyu.Zhang1@nottingham.ac.uk; david.gerada@nottingham.ac.uk).

working medium, which enhances the HP cooling effectiveness. Conversely, the return of the working medium will be hindered, and the HP thermal characteristic is thus weakened for the gravity-opposed case.

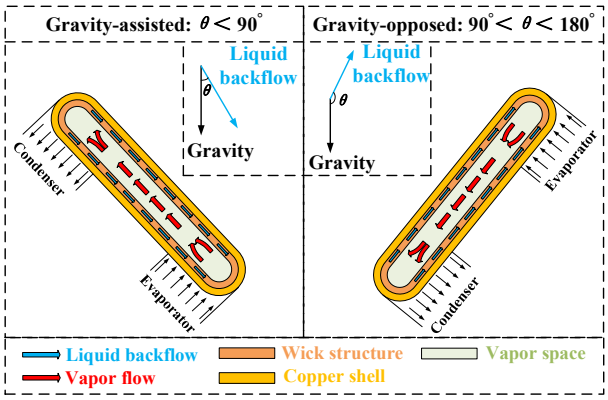

Fig. 2. Gravitational effect on the backflow of the internal working medium in the HP for the gravity-assisted case and gravity-opposed case.

When incorporated in motor cooling systems, HPs are generally installed uniformly into motor assemblies along the circumference, as presented in Fig. 3 [17-22], which intends to achieve a comparatively even working temperature distribution. In this case, HPs are with different inclination angles along the circumference and present various cooling capabilities, which result in a nonuniform temperature distribution. Such temperature difference may cause unexpected thermal stress or deformation and increase the stability-related risk.

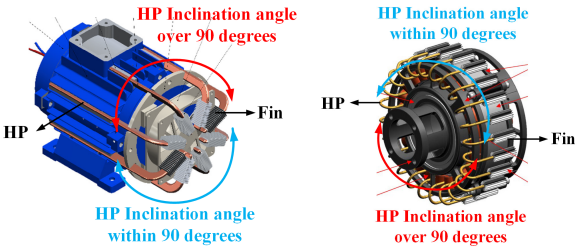

Fig. 3. HP applications in electrical machines with different inclination angles [21, 22].

The inclination angle effect of HPs in other application scenarios has been extensively investigated. In [23], the HP inclination angle effect on the performance of CPU coolers has been studied and the results indicate that CPU cooling performance is greatly affected beyond a threshold angle. Similar studies have been also performed for HP photovoltaic/thermal systems, which shows the HP performance is sensitive to the inclination angle, especially for wickless HPs [24]. Furthermore, the orientation effect on pulsating HPs has been also studied in [25, 26], and the results point out that pulsating HPs with lower thermal resistance enable a more uniform heat distribution under gravity-assisted operation. However, the impact of HP inclination angle on motor temperature distribution is still unclear and requires an intensive investigation.

In the previous study [27], the effect of HP inclination angle on motor temperature distribution has been preliminarily evaluated through thermal analysis. This paper aims to provide a thorough investigation into this issue, primarily focusing on theoretical analysis, updated thermal modeling and evaluation, and experimental validation. The major novelties and contributions of this manuscript are summarized as follows:

(i) An analytical model of the HP considering the inclination effect has been derived to clarify its impact mechanism.

(ii) The non-uniform motor temperature distribution due to the impact of HP inclination angle has been numerically investigated using a more precise modeling approach, together with its variation under different thermal loads and cooling conditions.

(iii) Experimental validation has been conducted to verify the thermal simulation results, including specimen preparation, experimental setup, and results analysis.

The remainder of this article is organized as follows. Section II theoretically analyzes the inclination angle effect on HP thermal performance. In Section III, a dedicated experimental setup is established and the HP equivalent thermal conductivities with different inclination angles are experimentally studied. Then, a 3-D thermal model based on a full-size stator-winding assembly is developed and motor temperature distribution under different cooling methods is evaluated in Section IV. Section V experimentally verifies the thermal simulation results by testing on a prepared specimen. Finally, a conclusion is drawn in section VI.

II. Theoretical Analysis

The copper-water HP with sintered wick structure is the most widely used in motor cooling scenarios due to its remarkable thermal performance, and thereby it was selected to investigate the inclination effect in this study. According to the HP working principle, the maximum capillary force generated in the wick structure must be greater than the total pressure drops in the HP, otherwise, the HP will dry out in the evaporator section [9]. The pressure drop consists of the following three parts: (i) the liquid flow pressure drop $\triangle P_l$ required to return the liquid from the condenser to the evaporator; (ii) the vapor flow pressure drop $\triangle P_v$ needed to drive the vapor to flow from the evaporator to the condenser; and (iii) the pressure resulted by the gravity of the working medium, $\triangle P_g$ depending on the HP inclination angle, which may be positive, zero or negative. When the inclination angle is within 90°, gravity assists the capillary force, and it is negative. In contrast, the gravitational effect is marked positive for the inclination angle greater than 90°. The above discussions can be expressed by [28]:

$$\begin{cases} \triangle P_{c\max} \geqslant \triangle P_l + \triangle P_v - \triangle P_g \ , \ \theta \in (0^\circ,\ 90^\circ) \\ \triangle P_{c\max} \geqslant \triangle P_l + \triangle P_v + \triangle P_g \ , \ \theta \in (90^\circ,\ 180^\circ) \end{cases} \quad (1)$$

$\triangle P_{cmax}$ is the maximum capillary pressure provided by the wick structure, which can be calculated as:

$$\triangle P_{c\max} = \frac{2\sigma}{r_p}\cos\alpha \quad (2)$$

It is assumed that the HP is operating stably, and both the vapor and liquid flow are laminar flows. The vapor pressure drop $\triangle P_v$ can be expressed as:

$$\triangle P_v = \frac{8\mu_v Q_{\max} l_{eff}}{\pi \rho_v A_v d_h^2 J} \quad d_h = \frac{2A_l}{C_l} \tag{3}$$

According to Darcy's law, the liquid pressure drop $\triangle P_l$ can be calculated as:

$$\triangle P_l = \frac{\mu_l Q_{\max} l_{eff}}{\varepsilon \rho_l A_w J} \tag{4}$$

Additionally, the gravity pressure can be formalized as:

$$\triangle P_g = \begin{cases} \rho_l g l \sin(90^\circ - \theta) & , \theta \in (0^\circ,\ 90^\circ) \\ \rho_l g l \sin(\theta - 90^\circ) & , \theta \in (90^\circ,\ 180^\circ) \end{cases} \tag{5}$$

Substituting equations (2), (3), (4), and (5) into equation (1), the maximum heat flux Q_{max} can be obtained as:

$$Q_{\max} = \begin{cases} \left[\frac{2\sigma\cos\alpha}{r_p} + \rho_l g l \sin(90^\circ - \theta)\right] \cdot \left[l_{eff}\left(\frac{8\mu_v}{\pi\rho_v A_v d_h^2 J} + \frac{\mu_l}{\varepsilon\rho_l A_w J}\right)\right]^{-1} & , \theta \in (0^\circ,\ 90^\circ) \\ \left[\frac{2\sigma\cos\alpha}{r_p} - \rho_l g l \sin(\theta - 90^\circ)\right] \cdot \left[l_{eff}\left(\frac{8\mu_v}{\pi\rho_v A_v d_h^2 J} + \frac{\mu_l}{\varepsilon\rho_l A_w J}\right)\right]^{-1} & , \theta \in (90^\circ,\ 180^\circ) \end{cases} \tag{6}$$

The maximum heat flux through the HP considering the installed inclination angle is derived based on its operating mechanism. It is found that the maximum heat transfer of the HP degrades with the increasing inclination angle, which thereby results in a gradual deterioration in the HP thermal performance. All the related symbols are defined in Table I.

TABLE I
NOMENCLATURE

Symbol	Concept
l_{eff}	HP equivalent length
l	HP total length
d_h	Hydraulic diameter of the wick structure
A_v	Cross area of the vapor space
A_w	Cross area of the wick structure
A	Cross area of the HP
ε	Permeability of the wick structure
C_l	Cross area of the liquid channel
A_l	Wetted perimeter of the liquid channel
ρ_v	Vapor density
ρ_l	Density of liquid working medium
J	Latent heat of working medium
μ_v	Kinetic viscosity of vapor
μ_l	Liquid viscosity
g	Gravitational acceleration
θ	HP Inclination angle
α	Contact angle
σ	Surface tension of liquid
r_p	Pore radius of wick
Q_{max}	Maximum heat flux through the HP
P	Heat load through the HP
T_e	Average temperature of the HP evaporator section
T_c	Average temperature of the HP condenser section
T_0	Coolant temperature at surface S_2
$\triangle T$	Temperature gap between the HP evaporator and condenser sections
$\triangle T_s$	Temperature gap across the whole assembly
T_{max}	The maximum temperature across the assembly
T_{min}	The minimum temperature across the assembly
σ	Standard deviation of the winding temperature
T_i	Average temperature corresponding to the ith winding module
T_{av}	Average temperature of the entire winding section
R_{HP}	HP thermal resistance
λ_{HP}	HP equivalent thermal conductivity
h	The convective heat transfer coefficient
h_{max}	The maximum convective heat transfer coefficient
V_{max}	The maximum wind velocity
q	Heat flux in the solving domain
ρ	Material density
c_p	Specific heat capacity of the material
λ	Thermal conductivity of the material
S_1, S_2	Boundary surfaces of the assembly

III. Experimental Investigation of the HP Thermal Properties at Various Inclination Angles

Generally, the experimental method is adopted to characterize the HP thermal properties with simple principle and accurate result [29]. A dedicated experimental platform is established and the equivalent thermal conductivities of HPs with different inclination angles from 0° to 180° are experimentally investigated.

A. PTCHE-based Specimen Preparation

Fig. 4 presents the preparation process of the specimen used to experimentally measure the HP equivalent thermal conductivity. The positive temperature coefficient heating element (PTCHE), also known as the self-regulating heater, is used as the heat source in the specimen, due to the merits of rapid warm-up and accurate temperature maintenance at a fixed input voltage, as illustrated in Fig. 4(a). Compared to motor copper windings, the PTCHE offers the following benefits: (i) more precise thermocouple locations and temperature measurement, thereby conducive to the accurate determination of HP thermal properties, i.e., temperature gap and thermal resistance; (ii) time-efficient in terms of specimen preparation and thermal test. The detailed parameters of the HP and PTCHE used in this study are listed in Table II and Table III.

The PTCHE and fin are attached to both ends of the HP as the heat source and heat sink, respectively, as shown in Fig. 4(b). The length of the fin arrays is chosen to be close to that of the PTCHE, as the HP offers favorable thermal performance when the length of the evaporator section approaches to that of the condenser section [30]. A high-performance thermal grease with favorable dielectric strength, i.e., IC diamond [31], is used to enhance heat transfer and insulation performance at the

contact interfaces between HP and PTCHE, as well as HP and fin. For a more reliable connection, thermal adhesive is also applied to both ends of the contact interfaces to bond them together. Finally, multi-layer thermal insulation material (Nitrile rubber) is used to wrap the entire surface of the specimen except for the fin to minimize heat loss, as presented in Fig. 4(c). For a clear temperature profile along the specimen, four K-type thermocouples are affixed to different sections of the specimen with cyanoacrylate adhesive, where E_1 and E_2 are attached to the evaporator section, C_1 and C_2 are located at the condenser section, respectively. All the thermocouples are located on the centerline of the HP to ensure accurate temperature measurement.

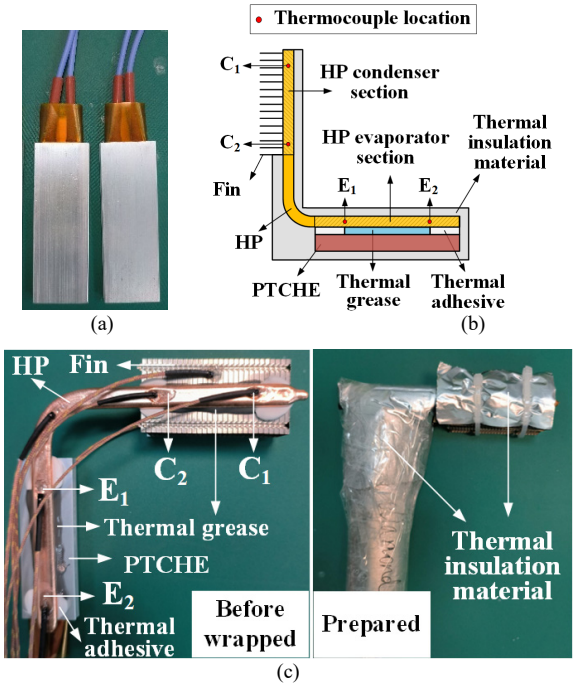

Fig. 4. PTCHE-based specimen preparation: (a) PTCHE. (b) Sketch for specimen preparation. (c) Prepared specimen.

TABLE II
HP PARAMETERS

Parameters	Value	Parameters	Value
Length	170 mm	Material	Copper
Width	8 mm	Working medium	Water
Thickness	3 mm	Wick structure	Sintered

TABLE III
PTCHE PARAMETERS

Parameters	Value	Parameters	Value
Input DC voltage	24 V	Length	60 mm
Steady-state temperature	110℃	Width	21 mm
Temperature deviation	± 10℃	Thickness	5 mm

B. Experimental Platform

An experimental platform based on the steady-state method is established to perform thermal tests on the prepared specimen [27], as presented in Fig. 5. The experimental specimen is affixed to the testbench by a clamp-on bench vise. For each inclination angle to be tested, the specimen is rotated to the specific angle, measured with a protractor and finally the vise is tightened to fix the specimen. A DC power supply (UTP 1310) is employed to provide the thermal load for the specimen, and its input power is measured by a power meter (YOKOGAWA WT333E). The air-cooling condition is realized by an electric fan which is placed on a height-adjustable platform. The position of the fan relative to the specimen is kept constant throughout the thermal test to ensure the same cooling environment. The temperature profile across the specimen is monitored by a thermal logger (Pico TC-08) and uploaded to the laptop for further statistics and analysis. Moreover, the wind velocity measured with an anemometer (OMEGA HHF144) is constant at 1m/s.

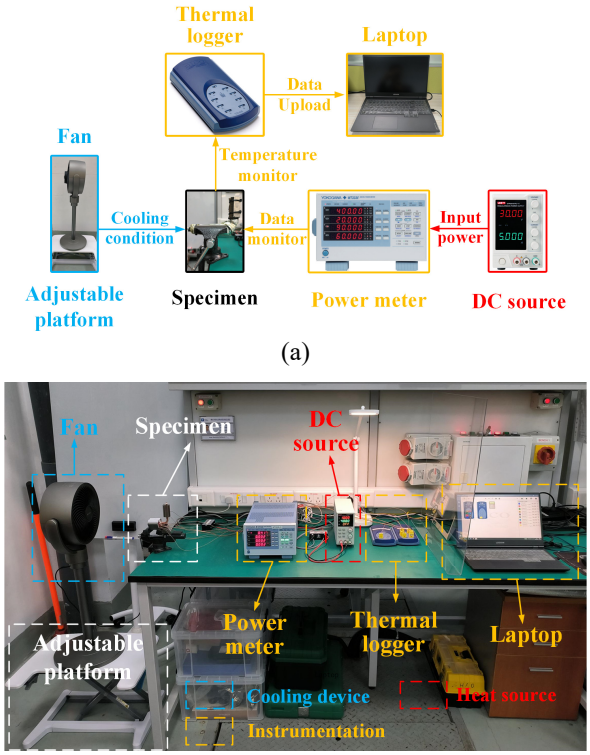

Fig. 5. Experimental platform for HP thermal properties. (a) Schematic. (b) Photo.

C. Data Processing

The HP thermal properties are characterized by the temperature gap $\triangle T$ between its evaporator and condenser sections, HP thermal resistance R_{HP}, and HP equivalent thermal conductivity λ_{HP} [30]. The temperature gap $\triangle T$ is given by:

$$\triangle T = T_e - T_c \tag{7}$$

where T_e and T_c are the average temperatures of the evaporator and condenser sections, which are calculated by:

$$T_e = \frac{T_{E1} + T_{E2}}{2},\ T_c = \frac{T_{C1} + T_{C2}}{2} \tag{8}$$

where T_{E1}, T_{E2}, T_{C1}, and T_{C2} are the temperature data measured

by the thermocouples E_1, E_2, C_1, and C_2. Thereby, the HP thermal resistance R_{HP} can be calculated by:

$$R_{HP} = \frac{\triangle T}{P} = \frac{T_e - T_c}{P} \tag{9}$$

where P is the heat load fed into the specimen, which is measured by the power meter. Finally, the HP equivalent thermal conductivity λ_{HP} can be obtained by:

$$\lambda_{HP} = \frac{l_{eff}}{R_{HP} A} = \frac{l_{eff} P}{(T_e - T_c) A} \tag{10}$$

where A is the cross-sectional area of the HP and l_{eff} is the equivalent length of the HP, i.e., the center-to-center distance of the HP evaporator and condenser sections.

D. Experiments and Results

During the thermal tests, the prepared specimen is affixed to the testbench with a clamp-on bench vise and oriented at an inclination angle from 0° to 180°, i.e., 0°, 30°, 60°, 90°, 120°, 150°, 180°), as presented in Fig. 6. All the tests are performed with the same input DC power and cooling conditions. The temperature data is logged every second throughout the experiment. When the temperature change is less than 0.2K within 5 minutes, thermal equilibrium is considered to be achieved and the sensor data are recorded.

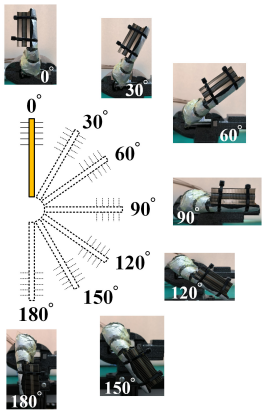

Fig. 6. HP orientation at different inclination angles.

Fig. 7 presents test results, i.e., the measured temperature gaps between the HP evaporator and condenser sections at various inclination angles. It can be clearly observed that the temperature gaps are comparatively small when the inclination angle changes from 0° to 90°, i.e., 0.4K to 0.6K, while increases significantly after the inclination angle above 90°, i.e., 0.87K to 2.25K.

Then, the HP thermal properties at various inclination angles, including thermal resistance and equivalent thermal conductivity, are calculated based on the above data processing method, as shown in Fig. 8. It can be observed that the HP presents favorable thermal performance with only a degradation of 31% in its thermal properties for gravity-assisted case ($\theta <$ 90°). However, the HP equivalent thermal conductivity deteriorates rapidly from more than 150000 W/m·K to less than 50000 W/m·K when the inclination angle exceeds 90°.

On this basis, the general variation pattern of HP equivalent thermal conductivity with its inclination angle can be obtained by fitting the measured data, as shown by the purple dashed line in Fig. 8. Mathematically, the variation can be described as:

$$\lambda_{HP}(\theta) = 273078.6 - 1243.5\theta,\ \theta \in (0^\circ, 180^\circ) \tag{11}$$

where θ is the inclination angle of the HP. The coefficient of determination of the fitting results is 0.99, which indicates that the approximation model has high accuracy, i.e., it can perfectly predict the HP equivalent thermal conductivities at various inclination angles.

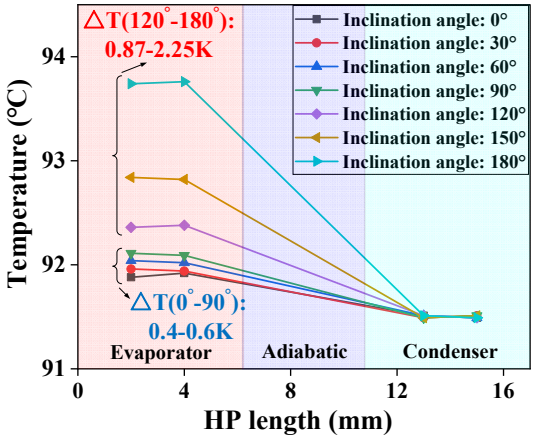

Fig. 7. Temperature gaps between the HP evaporator and condenser sections at various inclination angles.

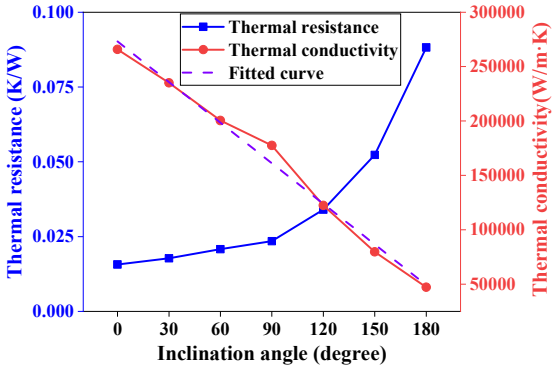

Fig. 8. HP thermal properties at various inclination angles.

IV. Thermal Modeling and Analysis

Based on the experimental studies of the HP thermal properties in Section III, the effects of inclination angle on motor temperature distribution are further quantitatively evaluated through thermal analysis on a full-size stator-winding assembly.

A. Stator-winding Assembly

As presented in Fig. 9, a full-size stator-winding assembly with HPs is developed for the evaluation of the HP inclination angle effect on motor temperature distribution. Copper wires are wounded on a stator stack with slot liner used for insulation. One end of the HPs is inserted into the clearance between winding layers, and the other end is equipped with aluminum fins as heat sink. The contact interfaces between HPs and windings are coated with the same thermal grease (IC diamond)

as the PTCHE-based specimens to enhance heat transfer and insulation performance. To facilitate data statistics and comparative analysis, HPs and adjacent windings are numbered clockwise along the circumference, as shown in Fig. 9.

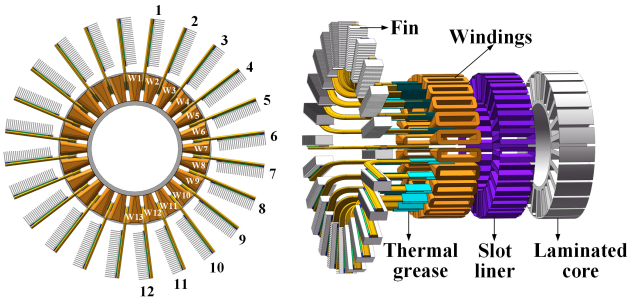

Fig. 9. Stator-winding assembly with HPs.

B. Mathematical Model

The heat transfer process of the motor assembly is theoretically governed by the energy conservation law [32]:

$$\rho c_p \frac{\partial T}{\partial t} = \nabla(\lambda \nabla T) + q \tag{12}$$

where q is the heat flux in the solving domain, ρ, c_p and λ are the density, specific heat capacity, and thermal conductivity of the materials in the assembly, respectively. In this study, the effect of thermal radiation is ignored, and heat convection occurs only at the fin surface. Therefore, the heat conduction equation for the transient temperature of a 3-D thermal model in Cartesian coordinates together with boundary conditions can be expressed as

$$\begin{cases} \rho c_p \dfrac{\partial T}{\partial t} = \dfrac{\partial}{\partial x}\left[\lambda_x \dfrac{\partial T}{\partial x}\right] + \dfrac{\partial}{\partial y}\left[\lambda_y \dfrac{\partial T}{\partial y}\right] \\ \qquad\qquad + \dfrac{\partial}{\partial z}\left[\lambda_z \dfrac{\partial T}{\partial z}\right] + q \\ \lambda \dfrac{\partial T}{\partial n}\Big|_{S_1} = q_0 \\ \lambda \dfrac{\partial T}{\partial n}\Big|_{S_2} = -h(T - T_0) \end{cases} \tag{13}$$

where S_1 and S_2 are boundary surfaces of the assembly, h is the convective heat transfer coefficient (CHTC) of the surface S_2, i.e., fin surface, T_0 is the coolant temperature at interface S_2, and q_0 is the heat flux through interface S_1. For an adiabatic surface, q_0 is zero.

C. Physical Model

A three-dimensional finite element analysis thermal model is established based on the proposed stator-winding assembly to quantitatively evaluate the effect of the HP inclination angle on the motor temperature distribution, as shown in Fig. 10. The heat transfer in the winding modules is critical and directly affects the accuracy of the motor thermal analysis results. The winding modules in electrical machines are generally considered to be anisotropic due to the insulating coating of the copper wires, the impregnating process of the winding section, and the air gaps between the wires. Therefore, the winding module is divided into in-slot winding and end winding for a clear temperature profile, where the heat is mainly transferred in the axial direction (along the z-axis) in the in-slot winding, while along the y-axis in the end winding [18, 33]. Moreover, the laminated core is also designated as an anisotropic material with heat transfer mainly along the radial direction (x-axis and y-axis). To facilitate mesh generation and calculational efficiency, the hollow multilayer HP based on the phase change principle is modeled as a solid copper rod with corresponding thermal property. The equivalent thermal conductivity at practical inclination angle is calculated by equation (11) and the results are listed in Table IV. Furthermore, the detailed thermal properties of the components involved in the thermal model are listed in Table V.

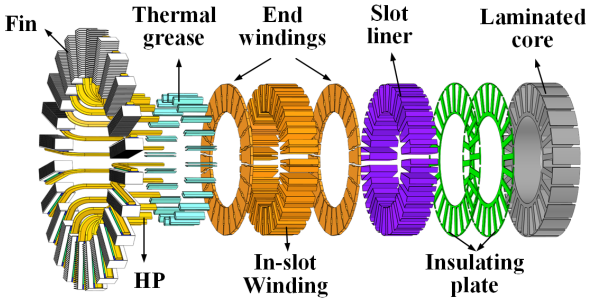

Fig. 10. Physical model of the stator-winding assembly with HPs.

TABLE IV
HP EQUIVALENT THERMAL CONDUCTIVITIES AT DIFFERENT INCLINATION ANGLES

Numbering_ Inclination Angle	Thermal Conductivity(W/m·K)	Numbering_ Inclination Angle	Thermal Conductivity (W/m·K)
1_7.5°	263752	7_97.5°	151837
2_22.5°	245100	8_112.5°	133185
3_37.5°	226447	9_127.5°	114532
4_52.5°	207795	10_142.5°	95880
5_67.5°	189142	11_157.5°	77227
6_82.5°	170490	12_172.5°	58575

TABLE V
THERMAL PROPERTIES OF COMPONENTS IN THE PHYSICAL MODEL [18, 34, 35]

Component	Material	Thermal Conductivity (W/m·K)
Laminated core	B50A350 silicon steel sheet	$\lambda_x = \lambda_y = 43$ $\lambda_z = 1.6$
In-slot Winding	QZY-2 (class F)	$\lambda_x = \lambda_y = 0.43$ $\lambda_z = 400$
End winding	QZY-2 (class F)	$\lambda_x = \lambda_z = 0.43$ $\lambda_y = 400$
Insulation board	Plastic (class F)	0.65
Slot liner	DMD insulation paper (class F)	0.3
Thermal grease	IC diamond	2000
Thermal adhesive	Silica gel	2
HP	Copper-water	Table IV
Fin	Aluminum	210

D. Boundary Conditions and Heat Sources

Generally, cooling methods for electrical machines can be classified into natural convection, forced convection and liquid cooling according to the fluid type and flow rate. Typical parameters for the above cooling methods are listed in Table VI, including the CHTC range and corresponding achievable current density intervals [36].

Heat sources and cooling conditions corresponding to the upper limits of the above typical value intervals are fed into the thermal model to evaluate the effect of HP inclination angle on the motor temperature distribution under different cooling methods. In the thermal model, the winding module is defined as the heat source, which is given the copper losses calculated from the winding phase resistance and the current data in Table VI. Whilst, fins are assigned as the heat sink with corresponding CHTC, as presented in Fig. 11.

TABLE VI
TYPICAL PARAMETERS FOR COMMON COOLING METHODS

Cooling Method	Current Density (A/mm^2)	CHTC (W/m^2·K)
Natural convection	1.5-5	5-10
Forced convection	5-10	10-300
Liquid cooling	10-30	50-20000

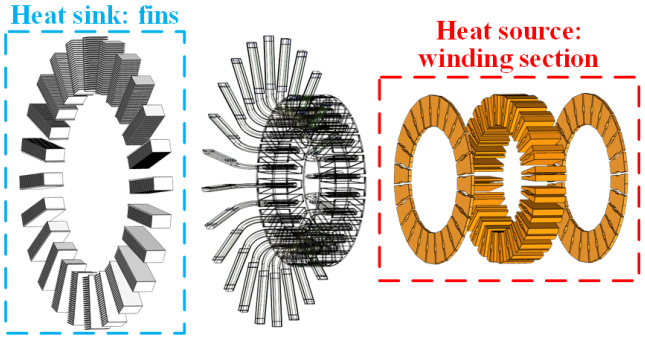

Fig. 11 Heat source and heat sink.

E. Results and Analysis

Thermal simulation of the stator-winding assembly is performed under natural convection, forced convection and liquid cooling, respectively, with results presented in Fig. 12.

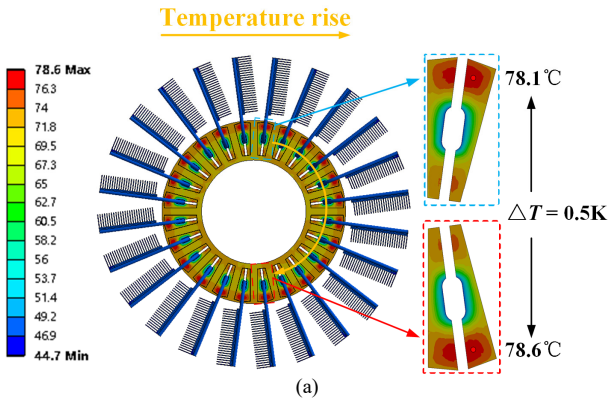

(a)

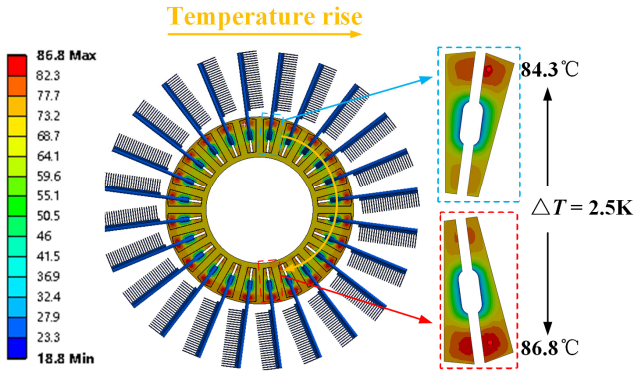

(b)

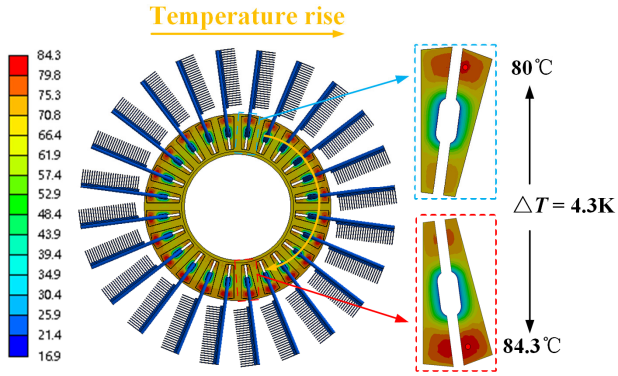

(c)

Fig. 12. Thermal analysis results under various cooling conditions. (a) Natural convection (5 A/mm^2 and 10 W/m^2·K). (b) Forced convection (10 A/mm^2 and 300 W/m^2·K) (c) Liquid cooling (30 A/mm^2 and 20000 W/m^2·K).

It can be seen that the temperature distribution pattern is similar under three cooling conditions, i.e., the winding temperature rises gradually with the increasing HP inclination angle. The hotspot appears in the winding section with the largest HP inclination angle (W13), while the lowest temperature occurs in the winding module with the smallest HP inclination angle (W1). The non-uniform temperature distribution becomes more pronounced with the increasing current density and cooling conditions, i.e., the temperature gap intensifies from 0.5K for natural convection to 4.3K for liquid cooling.

Based on the proposed thermal model, the effects of thermal load and cooling conditions on the non-uniform motor temperature distribution are further studied, with results presented in Fig. 13. It can be observed that the temperature gap increases considerably from natural convection to forced convection, while almost flat further to liquid cooling. The main reason is that the convective thermal resistance is reduced, and the ratio of HP thermal resistance in the cooling path is increased, which enhances HP inclination angle effect. Similar to the CHTC effect, the temperature nonuniformity deteriorates with the increasing current density, and the variation slows down beyond a threshold, which is mainly caused by the growing HP inclination angle effect due to the increasing heat flux.

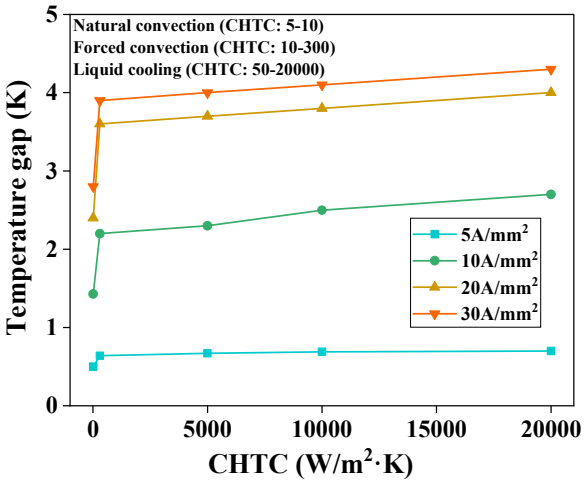

Fig. 13. Effects of current density and cooling conditions on motor temperature distribution, i.e., the temperature gap across the whole winding section.

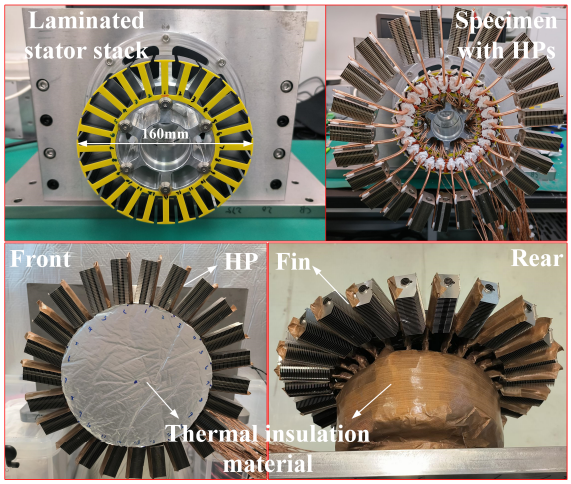

Fig. 14. Preparation process of the experimental specimen.

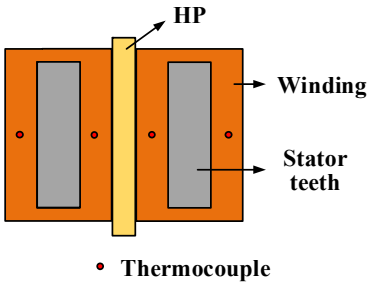

Fig. 15. Thermocouple location in winding modules.

V. Experimental Validation

The effects of HP inclination angle on motor temperature distribution are experimentally investigated in this section to verify the above thermal simulation results, with specimen preparation in Part A, and experimental setup in Part B, as well as results analysis in Part C.

A. Experimental Specimen Preparation

According to the proposed stator-winding assembly in Fig. 9, an experimental specimen featuring a 24-slot and an outer diameter of 160 mm is prepared, as presented in Fig. 14. Copper wires are wound on a laminated core in a concentrated layout with slot liner and insulation board used for insulation consideration. The same cooling components as the PTCHE-based specimen, including HPs and fins, are inserted uniformly into winding clearances along the circumference. High-performance thermal grease (IC diamond) is also applied to the contact interface between the HP and windings to enhance heat transfer and electric insulation. Furthermore, the entire specimen is wrapped with multi-layer thermal insulation material (Nitrile rubber) except for the fins to ensure that the heat generated is only dissipated by the HPs and fins, so as to fully evaluate the HP inclination angle effect on the motor temperature distribution. The prepared specimen is affixed to a dedicated iron bracket through an aluminum flange for thermal test.

For a clear temperature profile across the specimen, a total of 48 K-type thermocouples are installed in the in-slot windings with cyanoacrylate adhesive, half of which are located in the center of the winding module on the left side of the HP and the other half are mounted on the right side, as detailed in Fig. 15. The average winding temperature is used to characterize the thermal performance of the inserted HPs, which refers to the average value of the temperature data collected by the two thermocouples in each slot.

B. Experimental Setup and Experimental Process

A dedicated experimental platform is established to perform thermal tests on the prepared specimen, as shown in Fig. 16. The specimen is powered by an adjustable DC power supply (DSP1050-42WE), which operates in the constant current mode during the test. A high-power axial flow fan with large fan blades is employed to provide uniform cooling conditions for the specimen. Moreover, the position of the fan relative to the specimen is kept constant during tests to ensure the same cooling environment.

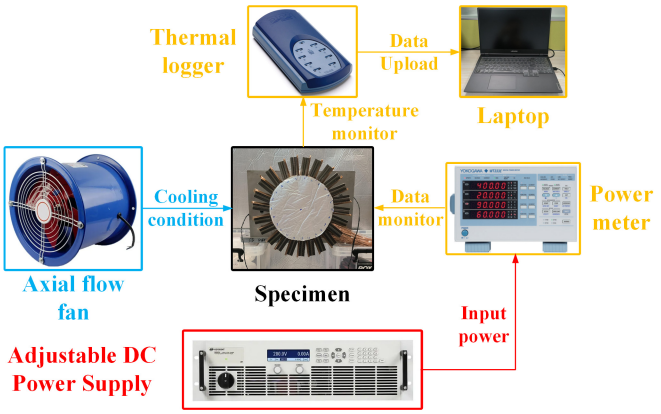

Fig. 16. Experimental setup.

Meanwhile, the experimental platform is equipped with a range of sensors and instrumentations to monitor the data required for further analysis, including electrical parameters,

temperature data, and wind velocity. A power meter (YOKOGAWA WT333E) is used to measure the thermal load fed into the specimen. The temperature profile across the specimen is monitored by thermal loggers (Pico TC-08). The temperature sensor readings are logged every second during the test. When the temperature variation is smaller than 0.2K within 5 minutes, thermal equilibrium is considered to be achieved and the sensors data are recorded. To ensure uniform cooling conditions, the wind velocities at eight monitoring points around the specimen are monitored by an anemometer (OMEGA HFF144), as detailed in Fig. 17. The deviation between the obtained data is less than 5%, which indicates uniform cooling conditions for the whole specimen.

Since the axial flow fan used in this study can only provide a maximum wind velocity of 7.5 m/s, the corresponding CHTC $h_{\max}$ can be calculated with the following empirical formula [18]:

$$h_{\max} = 28\left(1+\sqrt{0.45V_{\max}}\right) = 80 \ \text{W/m}^2\cdot\text{K} \qquad (14)$$

where $V_{\max}$ is the maximum wind speed that the fan can provide. Besides, the input heat source is adjusted to the power corresponding to a current density of 8 A/mm^2 to ensure that the winding temperature rise is within the permissible range of the wire insulation.

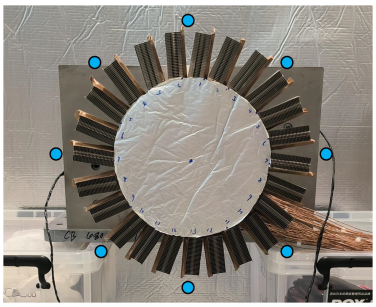

Fig. 17. Wind velocity monitoring points.

C. Results and Analysis

Temperature gap $\triangle T_s$ across the whole assembly and standard deviation σ of the winding temperature are used to characterize the motor temperature nonuniformity. The temperature gap $\triangle T_s$ refers to the difference between the maximum and minimum temperatures of the winding modules across the whole model, given by:

$$\triangle T_s = T_{\max} - T_{\min} \qquad (15)$$

Moreover, the standard deviation σ of the winding temperature is defined as:

$$\sigma = \sqrt{\sum_{i=1}^{n}(T_i - T_{av})^2/n} \qquad (16)$$

where n refers to the number of the winding module in Fig. 9, T_i is the average temperature corresponding to the ith winding module, and T_{av} is the average temperature of the entire winding section. The above parameters $\triangle T$ and σ are in K (Kelvin), while T_i and T_{av} are in ℃ (Celsius).

Fig. 18 presents the comparison of simulated and tested temperatures under a current density of 8 A/mm^2 and CHTC of 80 W/m^2·K. It can be observed from the experimental results that the winding temperature gradually rises with the increasing inclination angle, which is consistent with the thermal analysis results. The temperature gaps (1.91K and 2.43K) and standard deviations (0.62K and 0.77K) obtained by thermal analyses and thermal tests are in good agreement, where the deviations are below 22%. Possible reasons for the slightly higher measured temperatures than the simulated data may lie in the following aspects:

(i) Deviation between CHTC calculated from empirical formula and the practical cooling conditions.

(ii) In this study, the input heat source for the thermal model is the loss density, which is the copper loss divided by the volume of the winding module. The difference between the volume of the winding model and the practical winding may lead to deviations of the heat source and motor temperature distribution.

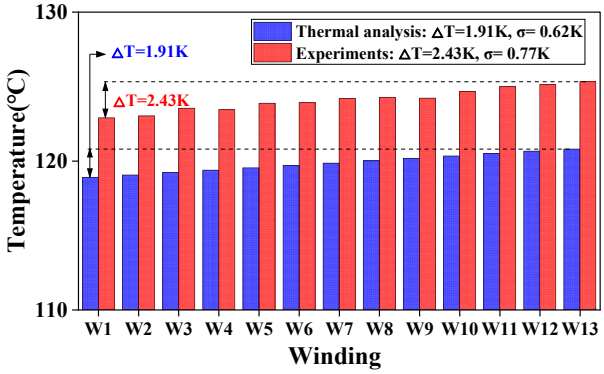

Fig. 18. Comparison of simulated and tested results under a current density of 8 A/mm^2 and CHTC of 80 W/m^2·K.

VI. Conclusion

HPs are being widely applied in motor cooling systems with remarkable cooling effects validated in the existing literature, while the effect of installed inclination angle on HP thermal characteristics and motor temperature distribution is still unclear and requires an intensive investigation.

In this article, the effects of HP inclination angle on its practical thermal performance and installed motor temperature distribution have been quantitatively studied. According to the experimental investigations on the PTCHE-based specimen, the HP equivalent thermal conductivity decreases by 31% when the inclination angle is within 90° while degrades up to 80% over 90°. Referring to the research findings of the full-size stator-winding assembly, the temperature nonuniformity deteriorates significantly with enhanced current density and cooling conditions. The temperature difference is only 0.5K under natural convection while increases to 4.3K under liquid cooling conditions and heavy thermal load, which needs to be fully considered when using HPs in motor cooling systems.

The quantitative analysis results obtained in this study could serve as guidelines for HP generalization in motor cooling scenarios. As for the potential research work, the impact of HP inclination angle in a practical motor can be further investigated

with full consideration of eddy current losses and motor operating duties.

REFERENCES

[1] C. Dong, Y. Qian, Y. Zhang, and W. Zhuge, "A Review of Thermal Designs for Improving Power Density in Electrical Machines," *IEEE Transactions on Transportation Electrification,* vol. 6, no. 4, pp. 1386-1400, 2020, doi: 10.1109/tte.2020.3003194.

[2] F. Zhang *et al.*, "Back-iron extension thermal benefits for electrical machines with concentrated windings," *IEEE Transactions on Industrial Electronics,* vol. 67, no. 3, pp. 1728-1738, 2019.

[3] F. Zhang *et al.*, "Slot Number Thermal Effects on Electrical Machines," *IEEE Transactions on Energy Conversion,* 2020.

[4] M. F. Palangar, A. Mahmoudi, S. Kahourzade, and W. L. Soong, "Electromagnetic and Thermal Analysis of a Line-Start Permanent-Magnet Synchronous Motor," in *2020 IEEE Energy Conversion Congress and Exposition (ECCE)*, 11-15 Oct. 2020 2020, pp. 502-508, doi: 10.1109/ECCE44975.2020.9235632.

[5] M. F. Palangar, A. Mahmoudi, S. Kahourzade, and W. L. Soong, "Optimum Design of Line-Start Permanent-Magnet Synchronous Motor Using Mathematical Method," in *2020 IEEE Energy Conversion Congress and Exposition (ECCE)*, 11-15 Oct. 2020 2020, pp. 2064-2071, doi: 10.1109/ECCE44975.2020.9236205.

[6] R. Wrobel and R. J. McGlen, "Opportunities and Challenges of Employing Heat-Pipes in Thermal Management of Electrical Machines," in *2020 International Conference on Electrical Machines (ICEM)*, 23-26 Aug. 2020 2020, vol. 1, pp. 961-967, doi: 10.1109/ICEM49940.2020.9270932.

[7] Z. Chen, Z. Yu, J. Fu, and B. Liu, "Study of heat pipe in motor cooling: A review," in *E3S Web of Conferences*, 2021, vol. 261: EDP Sciences.

[8] H. Zhao, X. Zhang, J. Li, L. Xu, S. Wang, and H. Zhang, "An Advanced Propulsion Motor with Enhanced Winding Cooling System for A Solar-Powered Aircraft," *IEEE Transactions on Transportation Electrification,* pp. 1-1, 2023, doi: 10.1109/TTE.2023.3285608.

[9] A. Faghri, "Heat Pipes: Review, Opportunities and Challenges," *Frontiers in Heat Pipes,* vol. 5, no. 1, 2014, doi: 10.5098/fhp.5.1.

[10] H. Zhao *et al.*, "A Comprehensive Review and Experimental Investigation on Heat Pipes Application in Electrical Machines," *IEEE Transactions on Transportation Electrification,* pp. 1-1, 2022, doi: 10.1109/TTE.2022.3207504.

[11] S. Noie, M. Sarmasti Emami, and M. Khoshnoodi, "Effect of inclination angle and filling ratio on thermal performance of a two-phase closed thermosyphon under normal operating conditions," *Heat transfer engineering,* vol. 28, no. 4, pp. 365-371, 2007.

[12] A. A. Alammar, R. K. Al-Dadah, and S. M. Mahmoud, "Numerical investigation of effect of fill ratio and inclination angle on a thermosiphon heat pipe thermal performance," *Applied Thermal Engineering,* vol. 108, pp. 1055-1065, 2016.

[13] T. Yousefi, S. Mousavi, B. Farahbakhsh, and M. Saghir, "Experimental investigation on the performance of CPU coolers: Effect of heat pipe inclination angle and the use of nanofluids," *Microelectronics Reliability,* vol. 53, no. 12, pp. 1954-1961, 2013.

[14] Y. Ma *et al.*, "Effect of inclination angle on the startup of a frozen sodium heat pipe," *Applied Thermal Engineering,* vol. 201, p. 117625, 2022.

[15] T. Zhang, W. Zheng, L. Wang, Z. Yan, and M. Hu, "Experimental study and numerical validation on the effect of inclination angle to the thermal performance of solar heat pipe photovoltaic/thermal system," *Energy,* vol. 223, p. 120020, 2021.

[16] R. Kothari, S. K. Sahu, S. I. Kundalwal, and S. Sahoo, "Experimental investigation of the effect of inclination angle on the performance of phase change material based finned heat sink," *Journal of Energy Storage,* vol. 37, p. 102462, 2021.

[17] C. Dong, X. Hu, Y. Qian, W. Zhuge, and Y. Zhang, "Thermal Management Integrated with Flat Heat Pipes for In-Slot Stator Windings of Electric Motors," *IEEE Transactions on Industry Applications,* pp. 1-12, 2022, doi: 10.1109/TIA.2022.3204239.

[18] Z. Yu, Y. Li, Y. Jing, and J. Wang, "Cooling System of Outer Rotor SPMSM for a Two-Seater All-Electric Aircraft Based on Heat Pipe Technology," *IEEE Transactions on Transportation Electrification,* pp. 1-1, 2021, doi: 10.1109/TTE.2021.3127555.

[19] W. Geng, T. Zhu, Q. Li, and Z. Zhang, "Windings Indirect Liquid Cooling Method for a Compact Outer-Rotor PM Starter/Generator with Concentrated Windings," *IEEE Transactions on Energy Conversion,* pp. 1-1, 2021, doi: 10.1109/TEC.2021.3084507.

[20] R. Wrobel and D. Reay, "A Feasibility Study of Heat Pipes for Thermal Management of Electrical Machines," in *2020 IEEE Energy Conversion Congress and Exposition (ECCE)*, 11-15 Oct. 2020 2020, pp. 4230-4237, doi: 10.1109/ECCE44975.2020.9236391.

[21] N. Putra and B. Ariantara, "Electric motor thermal management system using L-shaped flat heat pipes," *Applied Thermal Engineering,* vol. 126, pp. 1156-1163, 2017, doi: 10.1016/j.applthermaleng.2017.01.090.

[22] X. Zhang, "A Novel Cooling Technique for the Windings of High-Torque-Density Permanent Magnet Machines," 2018.

[23] T. Yousefi, S. A. Mousavi, B. Farahbakhsh, and M. Saghir, "Experimental investigation on the performance of CPU coolers: Effect of heat pipe inclination angle and the use of nanofluids," *Microelectronics Reliability,* vol. 53, no. 12, pp. 1954-1961, 2013.

[24] M. Hu, R. Zheng, G. Pei, Y. Wang, J. Li, and J. Ji, "Experimental study of the effect of inclination angle on the thermal performance of heat pipe photovoltaic/thermal (PV/T) systems with wickless heat pipe and wire-meshed heat pipe," *Applied Thermal Engineering,* vol. 106, pp. 651-660, 2016.

[25] S. A. Jahan, M. Ali, and M. Q. Islam, "Effect of inclination angles on heat transfer characteristics of a closed loop pulsating heat pipe (CLPHP)," *Procedia Engineering,* vol. 56, pp. 82-87, 2013.

[26] F. Shang, S. Fan, Q. Yang, and J. Liu, "An experimental investigation on heat transfer performance of pulsating heat pipe," *Journal of Mechanical Science and Technology,* vol. 34, no. 1, pp. 425-433, 2020.

[27] H. Zhao, X. Zhang, X. Zhu, Y. Zhang, H. Yan, and Z. Niu, "Research on the Effect of Heat Pipe Inclination Angle on Temperature Distribution in Electrical Machines," in *2022 IEEE Transportation Electrification Conference and Expo, Asia-Pacific (ITEC Asia-Pacific)*, 28-31 Oct. 2022 2022, pp. 1-6, doi: 10.1109/ITECAsia-Pacific56316.2022.9941772.

[28] D. Reay, R. McGlen, and P. Kew, *Heat pipes: theory, design and applications*. Butterworth-Heinemann, 2013.

[29] T. A. Moreira, A. R. A. Colmanetti, and C. B. Tibirica, "Heat transfer coefficient: a review of measurement techniques," *Journal of the Brazilian Society of Mechanical Sciences and Engineering,* vol. 41, no. 6, pp. 1-25, 2019.

[30] S. Zhang *et al.*, "Experimental study on the thermal performance of a novel ultra-thin aluminum flat heat pipe," *Renewable Energy,* vol. 135, pp. 1133-1143, 2019.

[31] H. Zhao *et al.*, "Effectiveness of Thermal Interface Materials on Electrical Machines Thermal Performance with Heat Pipes," *IEEE Transactions on Transportation Electrification,* pp. 1-1, 2023, doi: 10.1109/TTE.2023.3274554.

[32] G. Fang, W. Yuan, Z. Yan, Y. Sun, and Y. Tang, "Thermal management integrated with three-dimensional heat pipes for air-cooled permanent magnet synchronous motor," *Applied Thermal Engineering,* vol. 152, pp. 594-604, 2019.

[33] W. Le *et al.*, "A Novel Stator Cooling Structure for Yokeless and Segmented Armature Axial Flux Machine with Heat Pipe," *Energies,* vol. 14, no. 18, p. 5717, 2021.

[34] H. Zhao *et al.*, "Heat Pipe Bending Effect on Cooling Effectiveness in Electrical Machines," *IEEE Transactions on Energy Conversion,* pp. 1-11, 2023, doi: 10.1109/TEC.2023.3249971.

[35] M. F. Palangar, W. L. Soong, and A. Mahmoudi, "Outer and Inner Rotor Line-Start Permanent-Magnet Synchronous Motors: An Electromagnetic and Thermal Comparison Study," in *2021 IEEE Energy Conversion Congress and Exposition (ECCE)*, 10-14 Oct. 2021 2021, pp. 4226-4233, doi: 10.1109/ECCE47101.2021.9595574.

[36] Y. Gai *et al.*, "Cooling of Automotive Traction Motors: Schemes, Examples, and Computation Methods," *IEEE Transactions on Industrial Electronics,* vol. 66, no. 3, pp. 1681-1692, 2019, doi: 10.1109/tie.2018.2835397.

Han Zhao was born in Heilongjiang, China. He received the B.Eng. and M.Eng. degrees in electrical engineering from the Harbin Institute of Technology, Harbin, China, in 2012 and 2014, respectively. He is currently working toward the Ph.D. degree within the Key Laboratory of More Electric

Aircraft Technology of Zhejiang Province at the University of Nottingham Ningbo China, Ningbo, China.

His main research interests include electromagnetic and thermal analysis on electrical machines for electric propulsion applications.

Mr. Han Zhao has been awarded Best Presentation Prizes at ICIT 2022 and ITEC Asia-Pacific 2022, respectively. The major research findings during his Ph.D. have been awarded first prize in Ningbo Innovation in Science and Technology Competition.

Xiaochen Zhang received the master's degree from Harbin University of Science and Technology, Harbin, China, in 2006, and the Ph.D. degree from Harbin Institute of Electrical Technology, Harbin, in 2012.

He is with the Yongjiang Laboratory, and the University of Nottingham Ningbo China, Ningbo, China. His research interests include research on electromagnetic and thermal analysis on electrical machine, especially in permanent magnetic machines and high-speed machines.

Dr. Xiaochen Zhang is a fellow of the Royal Aeronautical Society (FRAeS).

Jing Li received the B.Eng. and M.Sc. degrees (Hons.) from the Beijing Institute of Technology, Beijing, China, in 1999 and 2002, respectively, and the Ph.D. degree from the University of Nottingham, Nottingham, U.K., in 2010, all in electrical and electronic engineering.

She was a Research Fellow after graduation with the Power Electronics, Machine and Control Group, University of Nottingham. In 2016, she joined the University of Nottingham Ningbo China, Ningbo, China, as an Assistant Professor, where she is currently an Associate Professor with the Department of Electrical and Electronic Engineering. Her research interests include condition monitoring for motor drive systems and power distribution systems, advanced control, and design of motor drive systems.

Fengyu Zhang received the B.E. degree in thermal engineering from Huazhong University of Science and Technology, Wuhan, China, in 2014, and the Ph.D. degree in electrical machines from the University of Nottingham, Nottingham, U.K., in 2019.

She is currently a Research Fellow in thermal management on electrical machines within the Power Electronics, Machines and Control (PEMC) Group, University of Nottingham. Her main research interests include high-performance motors for transport applications and their multidomain optimization.

Yue Zhang was born in Fujian, China, 2003. She is currently working toward B.Eng. degree in Electrical and Electronic Engineering from the University of Nottingham Ningbo China. She is also within the Key Laboratory of More Electric Aircraft Technology of Zhejiang Province at the University of Nottingham Ningbo China, Ningbo, China.

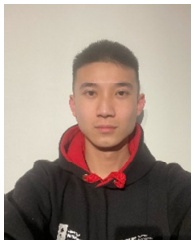

Hongyu Yan was born in Hubei, China, 2002. He is currently working toward B.Eng. degree in Electrical and Electronic Engineering from the University of Nottingham Ningbo China. He is also within the Key Laboratory of More Electric Aircraft Technology of Zhejiang Province at the University of Nottingham Ningbo China, Ningbo, China.

Xiaorui Zhu was born in Shandong, China, 2001. He is currently working toward B.Eng. degree in Electrical and Electronic Engineering from the University of Nottingham Ningbo China. He is also within the Key Laboratory of More Electric Aircraft Technology of Zhejiang Province at the University of Nottingham Ningbo China, Ningbo, China.

Zhihao Niu was born in Shanxi, China, 2002. He is currently working toward B.Eng. degree in Aerospace Engineering from the University of Nottingham Ningbo China. He is also within the Key Laboratory of More Electric Aircraft Technology of Zhejiang Province at the University of Nottingham Ningbo China, Ningbo, China.

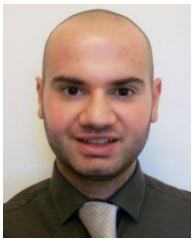

David Gerada received the Ph.D. degree in high-speed electrical machines from University of Nottingham, Nottingham, U.K., in 2012.

From 2007 to 2016, he was with the R&D Department, Cummins, Stamford, U.K., first as an Electromagnetic Design Engineer from 2007 to 2012, and then as a Senior Electromagnetic Design Engineer and Innovation Leader from 2012 to 2016. At Cummins, he pioneered the design and development of high-speed electrical machines, transforming a challenging technology into a reliable one suitable for the transportation market, while establishing industry-wide-used metrics for such machinery. In 2016, he joined the University of Nottingham where he is currently a Principal Research Fellow, responsible for developing state-of-the-art electrical machines for future transportation which push existing technology boundaries, while propelling the new technologies to higher technology readiness levels.

Dr. Gerada is a Chartered Engineer in the U.K. and a member of the Institution of Engineering and Technology.